Spectra in the Unstable Surface Layer

L. J. PELTIER

Department of Meteorology, The Pennsylvania State University, University Park, Pennsylvania

J. C. WYNGAARD

Departments of Meteorology and Mechanical Engineering, The Pennsylvania State University, University Park, Pennsylvania

S. KHANNA

Department of Mechanical Engineering, The Pennsylvania State University, University Park, Pennsylvania

J. G. BRASSEUR

Department of Mechanical Engineering, The Pennsylvania State University, University Park, Pennsylvania

(Manuscript received 19 September 1994, in final form 20 April 1995)

ABSTRACT

A simple approach to modeling spectra in unstable atmospheric surface layers is presented. The authors use a single form for the two-dimensional spectrum of horizontal velocity, vertical velocity, and a scalar in the horizontal plane; it has two free constants, a length scale, and an intensity scale. Continuity is used to relate the vertical and horizontal velocity spectra. The two free constants are determined by matching the variance and the inertial-subrange spectral level with observations. The scales are chosen so that the spectra follow law of the wall and mixed-layer scaling in the neutral and free-convection limits, respectively. The authors model the stability dependence of the spectra by combining these two limiting forms. The one-dimensional spectra, obtained by integration over one wavenumber component, and their variances agree well with observations. Near the surface the vertical velocity variance follows Monin–Obukhov (M–O) similarity and shows a realistic local free-convection asymptote; at greater heights it shows departures from M–O similarity that also agree well with observations. Finally, the two-dimensional spectra are used to calculate the variances of the resolvable and subgrid-scale components of large eddy simulations and their dependence on grid mesh size, distance from the surface, boundary layer depth, and stability.

1. Introduction

If its grid mesh is sufficiently fine, large-eddy simulation (LES) can produce resolvable-scale velocity and scalar constituent fields that replicate well the energy-containing-range structure of the atmospheric boundary layer. One exception is the region adjacent to the surface. Observations (Kaimal et al. 1976; Kaimal 1978) show that the horizontal scales of vertical (w) and horizontal (u, v) velocity fluctuations behave quite differently in this surface layer. For example, in unstable conditions, the horizontal scale of w is proportional to distance from the surface z, while the horizontal scale of u and v is proportional to the boundary-layer depth z_i. It follows that LES with a fixed horizontal grid mesh Δ will resolve the w-field poorly close to the surface, but since typically $\Delta \ll z_i$, it can resolve the u and v fields there quite well.

This discussion suggests that the amplitude of a resolvable-scale field within the surface layer depends in general on the cutoff wavenumber (which is inversely proportional to the LES grid size Δ) and boundary-layer depth z_i as well as on the traditional Monin–Obukhov (M–O) scaling parameters. In principle one can determine the Δ dependence through knowledge of the horizontal wavenumber spectrum of the variable, since the variance of its resolvable-scale part is the integral of this spectrum from zero to the cutoff wavenumber. Thus, one needs a model of this horizontal wavenumber spectrum in the surface layer.

Previous efforts to model surface-layer spectra fall into two distinct categories. The first [as summarized by Panofsky and Dutton (1984), for example] deals directly with the one-dimensional streamwise wavenumber spectrum, which can be inferred from frequency spectra of measured time series through Tay-

Corresponding author address: Dr. Leonard Joel Peltier, Dept. of Meteorology, The Pennsylvania State University, 503 Walker Building, University Park, PA 16802-5013.
E-mail: peltier@essc.psu.edu

lor's frozen field hypothesis. The stability dependence of these spectra is typically modeled by superimposing the behavior seen in the neutral and convective limits (e.g., Højstrup 1982). Efforts falling into the second category have posed the problem in its full three-dimensionality, that is, in terms of the spectral density tensor as a function of three-dimensional wavenumber. Kristensen et al. (1989) used this approach with the assumption of homogeneity in all three directions, while Mann (1994) has allowed inhomogeneity in the vertical.

We use yet a different approach, one that combines much of the simplicity of the first with the sounder basis of the second. We focus on the two-dimensional spectra in the horizontal plane. This allows us to use two constraints: continuity, which couples the spectra of horizontal and vertical velocities, and isotropy in the horizontal plane in the free-convection limit, which imposes additional structural constraints on these spectra. We model stability effects through the superposition technique and then obtain the one-dimensional spectrum by integration over one wavenumber.

2. Turbulence in the surface layer

a. Fourier representation

Because surface-layer turbulence is inhomogeneous in the vertical (x_3 or z) direction, we use the Fourier representation in the horizontal directions only. Thus, we write the fluctuating parts of the velocity and conservative scalar fields as

$$u_i(x_i, t) = \int e^{i(\kappa_1 x_1 + \kappa_2 x_2)} dZ_i(\kappa_1, \kappa_2, z, t),$$

$$c(x_i, t) = \int e^{i(\kappa_1 x_1 + \kappa_2 x_2)} dC(\kappa_1, \kappa_2, z, t), \quad (1)$$

where $dZ_i\,(i = 1, 2, 3)$ and dC are the Fourier–Stieltjes components (Batchelor 1960; Lumley and Panofsky 1964). We define a spectral density tensor for velocity and a spectral density for the scalar as

$$\phi_{ij}(\kappa_1, \kappa_2, z, t)d\kappa_1 d\kappa_2 = \overline{dZ_i(\kappa_1, \kappa_2, z, t)dZ_j^*(\kappa_1, \kappa_2, z, t)},$$

$$\psi(\kappa_1, \kappa_2, z, t)d\kappa_1 d\kappa_2 = \overline{dC(\kappa_1, \kappa_2, z, t)dC^*(\kappa_1, \kappa_2, z, t)}, \quad (2)$$

where the overbar denotes the expected value. The velocity and scalar covariances are integrals of these spectral densities; for example,

$$\overline{u_i u_j}(z, t) = \iint_{-\infty}^{\infty} \phi_{ij}(\kappa_1, \kappa_2, z, t)d\kappa_1 d\kappa_2,$$

$$\overline{c^2}(z, t) = \iint_{-\infty}^{\infty} \psi(\kappa_1, \kappa_2, z, t)d\kappa_1 d\kappa_2. \quad (3)$$

We will not regularly indicate the time or height dependence hereafter.

b. The free-convection limit

In free convection there is no preferred direction within the horizontal plane, so the fluctuating fields are in a state of "horizontal isotropy." In this state the scalar spectrum depends only on κ, the magnitude of the horizontal wavenumber vector:

$$\psi(\kappa_1, \kappa_2) = \frac{E_c(\kappa)}{2\pi\kappa}, \quad (4)$$

where $\kappa = (\kappa_1^2 + \kappa_2^2)^{1/2}$. The factor 2π appears so that $E_c(\kappa)$ integrates to the scalar variance:

$$\iint_{-\infty}^{\infty} \psi(\kappa_1, \kappa_2)d\kappa_1 d\kappa_2 = \int_0^{\infty} \left(\int_0^{2\pi} \frac{E_c(\kappa)}{2\pi\kappa} \kappa d\theta \right) d\kappa = \int_0^{\infty} E_c(\kappa)d\kappa = \overline{c^2}. \quad (5)$$

We call $E_c(\kappa)$ a two-dimensional spectrum, in analogy to the standard nomenclature in three-dimensional representation of turbulence.

The form of the horizontal components of ϕ_{ij} under horizontal isotropy can be determined by the method developed by Robertson (1940), which is widely used in three-dimensional turbulence (Batchelor 1960). When applied to the two velocity components in the horizontal plane the result is

$$\phi_{ij}(\kappa_1, \kappa_2) = \alpha(\kappa)\kappa_i\kappa_j + \beta(\kappa)\delta_{ij} \quad (i, j = 1, 2), \quad (6)$$

where α and β are functions only of κ. In three dimensions the continuity constraint $u_{i,i} = 0$ implies that $\kappa_i\phi_{ij} = 0$, which couples α and β. In two dimensions continuity introduces $\partial u_3/\partial x_3$, which is unknown, so the spectra of the horizontal velocities retain their dependence on two unknown functions:

$$\phi_{11}(\kappa_1, \kappa_2) = \alpha(\kappa)\kappa_1^2 + \beta(\kappa),$$

$$\phi_{22}(\kappa_1, \kappa_2) = \alpha(\kappa)\kappa_2^2 + \beta(\kappa). \quad (7)$$

However, the sum of ϕ_{11} and ϕ_{22} is a single function of κ,

$$\frac{\phi_{11} + \phi_{22}}{2} = \frac{\alpha(\kappa)\kappa^2}{2} + \beta(\kappa) \equiv \frac{E_h(\kappa)}{2\pi\kappa}, \quad (8)$$

where $E_h(\kappa)$ is a two-dimensional energy spectrum with the property

$$\iint_{-\infty}^{\infty} \left(\frac{\phi_{11} + \phi_{22}}{2} \right) d\kappa_1 d\kappa_2 = \int_0^{\infty} \left(\int_0^{2\pi} \frac{E_h(\kappa)}{2\pi\kappa} \kappa d\theta \right) d\kappa = \int_0^{\infty} E_h(\kappa)d\kappa = \frac{\overline{u_1^2} + \overline{u_2^2}}{2}. \quad (9)$$

c. Continuity and the vertical velocity spectrum

From (1) the continuity equation $u_{i,i} = 0$ implies that the Fourier–Stieltjes components for velocity satisfy

$$-i\kappa_1 dZ_1 - i\kappa_2 dZ_2 = \frac{\partial dZ_3}{\partial z}. \quad (10)$$

Integrating over height z gives

$$-i\kappa_1 \int_{z_0}^{z} dZ_1(\kappa_1, \kappa_2, z')dz' - i\kappa_2 \int_{z_0}^{z} dZ_2(\kappa_1, \kappa_2, z')dz' = dZ_3(\kappa_1, \kappa_2, z), \quad (11)$$

assuming that the velocity field vanishes at the roughness height z_0.

Consider the limit $\kappa z \ll 1$, that is, horizontal scales very large compared with distance from the surface. We now introduce a hypothesis through which the z-dependence of the Fourier coefficients in (11) can be deduced. We assume that the largest horizontal scales ($\kappa z \ll 1$) of the horizontal velocity field have the z-dependence of the mean wind profile $U(z)$:

$$U(z) = \frac{u_*}{k}\left(\ln\frac{z}{z_0} - \Psi(z/L)\right). \quad (12)$$

Here Ψ represents the stability correction to the logarithmic profile (Paulson 1970); k is the von Kármán constant; and $L = -u_*^3 T_0/kgQ_0$, with g/T_0 the buoyancy parameter and Q_0 the surface temperature flux, is the Monin–Obukhov length. In free convection, where $U = 0$, we interpret U as a random, local mean wind profile due to the largest convective eddies (Businger 1973). From (12) we can write

$$\int_{z_0}^{z} U(z')dz' = AzU(z), \quad (13)$$

where the parameter A depends on z/z_0 and z/L. Under neutral conditions ($z/L = 0$), Ψ vanishes and (13) yields $A = 1 + z_0/z - 1/\ln(z/z_0)$. Under convective conditions ($z/L < 0$) the mean wind shear decreases (Businger 1973) and $A \to 1.0$.

After applying (13) to the z-integrals of the Fourier coefficients of horizontal velocity, (11) becomes

$$-iAz(\kappa_1 dZ_1 + \kappa_2 dZ_2) \approx dZ_3. \quad (14)$$

Multiplying (14) by its complex conjugate and averaging yields a relation among the spectral density components at $\kappa z \ll 1$:

$$\phi_{33} \approx z^2A^2[\kappa_1^2\phi_{11} + \kappa_1\kappa_2[\phi_{12} + \phi_{21}] + \kappa_2^2\phi_{22}] \quad (\kappa z \ll 1). \quad (15)$$

Equation (15) may be interpreted in terms of the vertical component of vorticity,

$$\omega = \frac{\partial u_2}{\partial x_1} - \frac{\partial u_1}{\partial x_2}, \quad (16)$$

with Fourier–Stieltjes coefficients given by

$$\omega(x_i, t) = \int e^{i(\kappa_1 x_1 + \kappa_2 x_2)} d\Omega(\kappa_1, \kappa_2, z, t). \quad (17)$$

It follows that the Fourier–Stieltjes coefficients of vertical vorticity are related to those of horizontal velocity by

$$d\Omega = i\kappa_1 dZ_2 - i\kappa_2 dZ_1 \quad (18)$$

and that the spectral density of vertical vorticity

$$W(\kappa_1, \kappa_2)d\kappa_1 d\kappa_2 = \overline{d\Omega(\kappa_1, \kappa_2)d\Omega^*(\kappa_1, \kappa_2)} \quad (19)$$

is related to that of horizontal velocity by

$$W(\kappa_1, \kappa_2) = \kappa_1^2\phi_{22} - \kappa_1\kappa_2(\phi_{12} + \phi_{21}) + \kappa_2^2\phi_{11}. \quad (20)$$

By combining (15) and (20), we can write the horizontal spectrum of vertical velocity at $\kappa z \ll 1$ as

$$\phi_{33}(\kappa_1, \kappa_2) \approx z^2A^2\{\kappa^2[\phi_{11}(\kappa_1, \kappa_2) + \phi_{22}(\kappa_1, \kappa_2)] - W(\kappa_1, \kappa_2)\} \quad (\kappa z \ll 1). \quad (21)$$

We will argue in the next section that we need only the free-convection form of the continuity constraint (21). Thus, let us interpret it in the horizontally isotropic, free-convection limit. We define two-dimensional spectra for vertical velocity and vertical vorticity:

$$\phi_{33}(\kappa_1, \kappa_2) = \frac{E_v(\kappa)}{2\pi\kappa}, \quad \text{where} \quad \int_0^\infty E_v(\kappa)d\kappa = \overline{u_3^2}, \quad (22)$$

$$W(\kappa_1, \kappa_2) = \frac{E_\omega(\kappa)}{2\pi\kappa}, \quad \text{where} \quad \int_0^\infty E_\omega d\kappa = \overline{\omega^2}. \quad (23)$$

Using these expressions and (8), we can write (21) in the free-convection limit as

$$E_v \approx z^2A^2(2\kappa^2E_h - E_\omega) \quad (\kappa z \ll 1). \quad (24)$$

Figure 1 shows the terms on the right side of (24) as computed at $z = 10.4$ m from 96^3-point LES data [courtesy of C.-H. Moeng, National Center for Atmospheric Research (NCAR)] for free convection in the atmospheric boundary layer. In the range $\kappa z \ll 1$, E_ω is about an order of magnitude smaller than $2\kappa^2E_h(\kappa)$. Thus, to a good approximation, we can write the continuity constraint (24) in the free-convection limit as

$$E_v(\kappa) \approx 2A^2\kappa^2z^2E_h(\kappa) \quad (\kappa z \ll 1). \quad (25)$$

This says that near the surface and at the largest scales free-convection turbulence has much less energy in the vertical velocity than in the horizontal velocity.

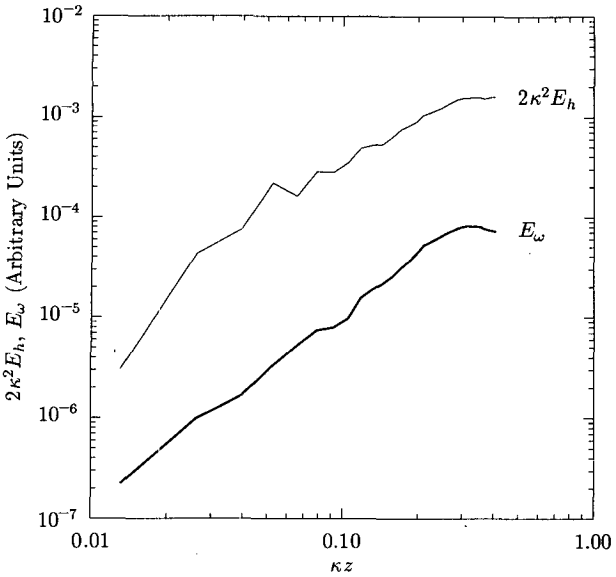

FIG. 1. The vertical vorticity spectrum $E_\omega(\kappa)$ compared with $2\kappa^2 E_h(\kappa)$, where E_h is the horizontal energy spectrum; see (24). (Data, courtesy of C.-H. Moeng, NCAR, are from $z = 10.4$ m in a 96^3 large-eddy simulation of free convection with $z_i = 1060$ m.)

3. Spectral modeling

a. Approach

Kaimal (1978) notes that in unstable surface layers $\overline{u_1^2} \approx \overline{u_2^2}$ and that their spectral shapes are quite similar as well. Thus, we will not distinguish between the u_1 and u_2 spectra; we will work instead with E_h.

We model the two-dimensional inertial spectra of horizontal energy, vertical velocity, and a conservative scalar with the single form

$$E(\kappa) = \frac{c_1 l^2 s^2 \kappa}{[c_2 + (\kappa l)^2]^{4/3}}. \tag{26}$$

This spectrum has a peak at $\kappa \sim 1/l$ and a $\kappa^{-5/3}$ inertial-range asymptote at $\kappa \gg l^{-1}$. It has four free parameters: the constants c_1 and c_2 and the characteristic length and intensity scales l and s.

We choose the scales l and s and the constants c_1 and c_2 separately for the neutral and free-convection states. We then combine these two limiting cases to give an interpolation formula for the entire stability range between them.

Our assumed form (26) is horizontally isotropic. This is rigorously valid for the free-convection state, but the neutral limit is horizontally anisotropic due to the mean wind shear. Thus, we define the two-dimensional spectra for neutral conditions (denoted with a superscript n) through the integral over circular rings in the horizontal wavenumber plane:

$$E_h^n(\kappa) = \int_0^{2\pi} \left(\frac{\phi_{11}^n + \phi_{22}^n}{2}\right)\kappa d\theta,$$

$$E_v^n(\kappa) = \int_0^{2\pi} \phi_{33}^n \kappa d\theta, \quad E_c^n(\kappa) = \int_0^{2\pi} \psi^n \kappa d\theta. \tag{27}$$

For application to vertical velocity under free convection (denoted with a superscript f), we modify our model (26) by taking E_v^f to be a filtered form of E_h^f:

$$E_v^f(\kappa) = T(\kappa, z) E_h^f(\kappa). \tag{28}$$

Here $T(\kappa, z)$ is a spectral transfer function that we will tailor to meet the continuity constraint (25) and to maintain the proper level in the inertial subrange.

If we compare our model form (26) for the two-dimensional spectrum of horizontal energy to the corresponding form derived from von Kármán's (1948) model for the three-dimensional energy spectrum (D. K. Wilson, personal communication 1994), we find that both are proportional to κ at small κ and $\kappa^{-5/3}$ at large κ. The transition between these limits, however, differs slightly. At low wavenumbers, our model slightly exceeds the von Kármán form for fixed inertial-range amplitudes. The one-dimensional spectra derived from these models are virtually indistinguishable.

Our form (26) does not include the mesoscale and synoptic-scale motions that do exist in the boundary layer. This neglect is consistent with the traditional notion of a "spectral gap" between shear and buoyancy-driven boundary-layer turbulence and the larger-scale noise (Lumley and Panofsky 1964). LES necessarily neglects these larger-scale components as well.

b. Determining the spectral parameters

Let us now consider the specification of the spectral constants and scales for horizontal energy and scalars. Because a transfer function is involved in the vertical velocity spectrum, we treat it separately.

1) THE CONSTANTS

We choose the spectral constants c_1 and c_2 such that the variance and the inertial subrange amplitude agree with observations. The variance contained in our model two-dimensional spectrum (26) is

$$\text{variance} = c_1 s^2 \int_0^\infty \frac{\kappa l}{[c_2 + (\kappa l)^2]^{4/3}} d(\kappa l) = \frac{3 c_1 s^2}{2 c_2^{1/3}}. \tag{29}$$

Measurements within the inertial range typically yield one-dimensional streamwise spectra. These are defined by

$$F_{ij}(\kappa_1) = 2\int_{-\infty}^{\infty} \phi_{ij}(\kappa_1, \kappa_2) d\kappa_2,$$

$$F_c(\kappa_1) = 2\int_{-\infty}^{\infty} \psi(\kappa_1, \kappa_2) d\kappa_2. \tag{30}$$

The factor of 2 in these definitions is not formally necessary but is typically used so that the integral of these one-dimensional spectra from 0 to ∞ is the variance.

Let us define the one-dimensional horizontal energy spectrum as

$$F_h(\kappa_1) = 2\int_{-\infty}^{\infty}\left(\frac{\phi_{11}+\phi_{22}}{2}\right)d\kappa_2 \equiv \frac{F_{11}+F_{22}}{2}. \quad (31)$$

In the horizontally isotropic free-convection limit we have

$$F_h^f(\kappa_1) = 2\int_{-\infty}^{\infty}\frac{E_h^f(\kappa)}{2\pi\kappa}d\kappa_2,$$

$$F_c^f(\kappa_1) = 2\int_{-\infty}^{\infty}\frac{E_c^f(\kappa)}{2\pi\kappa}d\kappa_2. \quad (32)$$

The neutral surface layer is not horizontally isotropic, so (32) is not valid there. However, we apply (32) in the neutral case as well, using for E the azimuthally averaged two-dimensional spectra defined in (27). This approximation reduces model complexity while retaining the essential coupling between one- and two-dimensional spectra. Thus, we write

$$F_h^n(\kappa_1) = 2\int_{-\infty}^{\infty}\frac{E_h^n(\kappa)}{2\pi\kappa}d\kappa_2,$$

$$F_c^n(\kappa_1) = 2\int_{-\infty}^{\infty}\frac{E_c^n(\kappa)}{2\pi\kappa}d\kappa_2. \quad (33)$$

The one-dimensional spectra corresponding to our model (26) of the two-dimensional spectrum are therefore

$$F_h(\kappa_1), F_c(\kappa_1)$$
$$= 2\left(\frac{1}{\pi}\int_0^{\pi/2}\cos^{2/3}x dx\right)\frac{c_1 l s^2}{[c_2+(l\kappa_1)^2]^{5/6}}$$
$$= \left[\frac{\pi^{-1/2}\Gamma(5/6)}{\Gamma(4/3)}\right]\frac{c_1 l s^2}{[c_2+(l\kappa_1)^2]^{5/6}}$$
$$= 0.71\frac{c_1 l s^2}{[c_2+(l\kappa_1)^2]^{5/6}}. \quad (34)$$

The inertial-range asymptote of (34) is

$$F_h(\kappa_1), F_c(\kappa_1) = 0.71 c_1 l^{-2/3} s^2 \kappa_1^{-5/3}. \quad (35)$$

In the inertial subrange the one-dimensional spectra are experimentally observed to follow the forms

$$F_{11}(\kappa_1) = \alpha_1\epsilon^{2/3}\kappa_1^{-5/3}, \quad F_{22}(\kappa_1) = \frac{4}{3}\alpha_1\epsilon^{2/3}\kappa_1^{-5/3},$$

$$F_c(\kappa_1) = \beta_1\epsilon^{-1/3}\chi\kappa_1^{-5/3}, \quad (36)$$

where α_1 and β_1 are the one-dimensional spectral constants and ϵ and χ are the molecular destruction rates of turbulent kinetic energy and scalar variance. The factor of 4/3 in F_2 is a consequence of three-dimensional local isotropy in the presence of a $-5/3$ power law. The notion of isotropy at inertial range and smaller scales in turbulent flows is now standard in turbulence applications, having its roots in Kolmogorov's (1941) work. There are some indications of fine-scale anisotropy in some flows, but these are principally of theoretical interest. Solving (35) and (36) for c_1 and (29) for c_2 then yields

$$c_1 = \frac{7\alpha_1}{6(0.71)}\left(\frac{\epsilon l}{s^3}\right)^{2/3} \quad \text{for horizontal energy,}$$

$$c_1 = \frac{\beta_1}{0.71}\left(\frac{\chi l^{2/3}}{\epsilon^{1/3}s^2}\right) \quad \text{for scalars,}$$

$$c_2 = \left(\frac{3c_1 s^2}{2\times\text{variance}}\right)^3. \quad (37)$$

2) THE SCALES

According to the law of the wall (e.g., Tennekes and Lumley 1972) the integral length scale in the neutral surface layer is proportional to z. The intensity scale (s) of horizontal velocity fluctuations is the friction velocity $u_* = (\tau_0/\rho)^{1/2}$, where τ_0 is the surface stress and ρ is density.

In free convection, velocity fluctuations away from the surface scale with $w_* = (gQ_0 z_i/T_0)^{1/3}$, where z_i is the convective-layer depth. It is now clear that these large, convective eddies also dominate the horizontal flow in the surface layer (e.g., Panofsky and Dutton 1984). Kaimal's (1978) observations show that the integral scale of horizontal velocity fluctuations near the surface scales with z_i, rather than z. Thus, for the horizontal energy spectrum under neutral conditions we take $l = z$, $s = u_*$; in free convection we take $l = z_i$, $s = w_*$.

We choose the scalar intensity scales (s) in the neutral and free-convection surface layers as

$$C_* = -\frac{\overline{wc}_0}{u_*}, \quad C_f = \frac{\overline{wc}_0}{u_f}. \quad (38)$$

Here, $\overline{wc}_0$ is the surface flux of the scalar, and u_f is the local free-convection velocity scale $(gQ_0 z/T_0)^{1/3}$. Temperature fluctuation measurements in laboratory free convection (Willis and Deardorff 1974) and in the very unstable surface layer (Wyngaard et al. 1971) support the choice of the local-free-convection intensity scale C_f. It is traditional to use a negative sign with C_* but not with C_f, as in (38). As with horizontal velocity, we take $l = z$ and $l = z_i$ in the neutral and free-convection limits, respectively.

c. Vertical velocity

In neutral conditions our assumed form (26) for $E(\kappa)$ peaks at $\kappa z \sim (3c_2/5)^{1/2} = O(1)$ and contains

negligible variance for $\kappa z \ll 1$. As a result, there is no need to apply the continuity constraint at $\kappa z \ll 1$, since $E(\kappa)$ is negligible there. Thus, we use the form (26) for E_v^n but choose its constants independently of E_h^n (appendix A).

Scales are generally much larger in free convection than in neutral conditions, so we need the continuity constraint in that limit. Because free convection is horizontally isotropic, the one-dimensional streamwise spectrum of vertical velocity is, from (22), (28), and (30),

$$F_{33}^f(\kappa_1) = 2\int_{-\infty}^{\infty} \frac{E_v^f(\kappa)}{2\pi\kappa}\, d\kappa_2 = 2\int_{-\infty}^{\infty} \frac{T(\kappa, z)E_h^f(\kappa)}{2\pi\kappa}\, d\kappa_2. \quad (39)$$

At small wavenumbers we use (25) to write the spectral transfer function $T(\kappa, z)$ as

$$T(\kappa, z) = 2A^2(\kappa z)^2 \quad (\kappa z \ll 1), \quad (40)$$

where A is the constant in (13). At large wavenumbers we satisfy three-dimensional local isotropy. In the inertial subrange, F_{33} behaves as

$$F_{33}(\kappa_1) = \frac{4}{3}\alpha_1 \epsilon^{2/3}\kappa_1^{-5/3}. \quad (41)$$

Thus, at $\kappa z \gg 1$, E_v^f must satisfy

$$E_v^f = \frac{8}{7}E_h^f, \quad (\kappa z \gg 1). \quad (42)$$

In consistency with (40) and (42) we model the spectral transfer function in (28) as

$$T(\kappa, z) = \frac{(\kappa z)^2}{\frac{1}{2A^2} + \frac{7}{8}(\kappa z)^2}, \quad (43)$$

which satisfies the continuity constraint at small κz and the inertial-range local isotropy constraint at large κz.

d. The composite spectra

Our scales for horizontal velocity, u_* at neutral and w_* in free convection, vanish in the opposite limit; that is, $u_* = 0$ in free convection and $w_* = 0$ at neutral. The simplest expression for the two-dimensional horizontal energy spectrum over this stability range that behaves properly in these two limits is the simple interpolation formula

$$E_h^m(\kappa) = E_h^n(\kappa) + E_h^f(\kappa), \quad (44)$$

where the superscript m denotes model. This simple model of the stability dependence implies that the horizontal velocity variance is the sum of the variances at neutral and in free convection. For our assumed spectral form and the chosen values of its constants (appendix A) this sum is

$$\sigma_h^2 = 12^{2/3}u_*^2 + 0.45w_*^2. \quad (45)$$

Using the identity $kw_*^3/u_*^3 = -z_i/L$, this can be written

$$\sigma_h^2 \approx u_*^2\left[12^{2/3} + 0.8\left(-\frac{z_i}{L}\right)^{2/3}\right]. \quad (46)$$

By contrast, the empirical form suggested by Panofsky et al. (1977) implies that the 3/2 powers of the variances add

$$\sigma_h^3 = 12u_*^3 + 0.2w_*^3, \quad (47)$$

which is equivalent to

$$\sigma_h^2 = u_*^2\left(12 - 0.5\frac{z_i}{L}\right)^{2/3}. \quad (48)$$

The Panofsky et al. (1977) expression (48) agrees with our result (45) at neutral but is about 20% smaller in free convection. Existing data are quite scattered, and the two forms seem to perform equally well.

Using the estimates of the constants given in appendix A, our model (44) yields for $z \gg z_0$

$$E_h^m(\kappa) = \frac{1.6z^2\kappa}{[0.091 + (\kappa z)^2]^{4/3}}u_*^2 + \frac{0.85z_i^2\kappa}{[23 + (\kappa z_i)^2]^{4/3}}w_*^2. \quad (49)$$

This model (49) of the horizontal energy spectrum does not follow M–O similarity. Its second term depends on the boundary layer depth z_i, which is not an M–O parameter. This is consistent with observations and can be quite important in applications (Wyngaard 1988). Its inertial range is M–O similar, however, because for wavenumbers such that $(\kappa z_i)^2 \gg 23$, (49) becomes independent of z_i.

The corresponding interpolation model for the vertical velocity spectrum is

$$E_v^m(\kappa) = E_v^n(\kappa) + T(\kappa, z)E_h^f(\kappa). \quad (50)$$

Using our estimates of the constants (appendix A), this gives

$$E_v^m(\kappa) = \frac{1.8z^2\kappa}{[5.2 + (\kappa z)^2]^{4/3}}u_*^2 + \frac{(\kappa z)^2}{\left[0.62 + \frac{7}{8}(\kappa z)^2\right]}\frac{0.85z_i^2\kappa}{[23 + (\kappa z_i)^2]^{4/3}}w_*^2. \quad (51)$$

Let us examine the departure from M–O similarity of the second term by using the identity $w_*^2 = u_f^2(z/z_i)^{-2/3}$ and rewriting (51) as

$$E_v^m(\kappa) = \frac{1.8z^2\kappa}{[5.2 + (\kappa z)^2]^{4/3}} u_*^2 + \frac{(\kappa z)^2}{\left[0.62 + \frac{7}{8}(\kappa z)^2\right]} \frac{0.85z^2\kappa}{[23(z/z_i)^2 + (\kappa z)^2]^{4/3}} u_f^2. \quad (52)$$

For $\kappa z \gg 1$ (i.e., at inertial-range wavenumbers) the z/z_i term in (52) is negligible, and our model vertical velocity spectrum is M–O similar. For $\kappa z \ll 1$, however, the z/z_i term is significant, and the spectrum deviates from M–O similarity.

The variance corresponding to our model spectrum (52) of vertical velocity is, for small z/z_i (appendix B),

$$\overline{u_3^2} = 1.6u_*^2 + \left[2 - 25\left(\frac{z}{z_i}\right)^{4/3}\right] u_f^2. \quad (53)$$

This can be written as

$$\overline{u_3^2} = u_*^2\left[1.6 + 3.7\left(-\frac{z}{L}\right)^{2/3} - 46\left(\frac{z}{z_i}\right)^{4/3}\left(-\frac{z}{L}\right)^{2/3}\right], \quad (54)$$

whose third term shows how $\overline{u_3^2}$ departs from M–O similarity. For $z/z_i \leq 0.03$ this departure is less than 12%.

The scalar intensity scales behave quite differently from those for velocity. The neutral scale C_* becomes infinite in free convection, and the free-convection scale C_f becomes infinite at neutral. It follows that the corresponding interpolation model for the scalar spectrum should involve the reciprocals of these scales. Thus, in the simplest model we add the scalar spectra in parallel:

$$\frac{1}{E_c^m(\kappa)} = \frac{1}{E_c^n(\kappa)} + \frac{1}{E_c^f(\kappa)}. \quad (55)$$

We use (55) with the neutral and free-convection forms (see appendix A):

$$E_c^n = \frac{1.5z^2\kappa}{[0.05 + (\kappa z)^2]^{4/3}} C_*^2,$$

$$E_c^f = \frac{0.77\left(\frac{z}{z_i}\right)^{-2/3} z_i^2\kappa}{\left[0.34\left(\frac{z}{z_i}\right)^{-2} + (\kappa z_i)^2\right]^{4/3}} C_f^2 = \frac{0.77z^2\kappa}{[0.34 + (\kappa z)^2]^{4/3}} C_f^2. \quad (56)$$

Equation (56) indicates that E_c^f is independent of the boundary-layer depth z_i and, hence, is M–O similar, despite our having chosen $l \sim z_i$ in the model spectrum (26) in the free-convection limit. The loss of z_i dependence in (56) stems from our specification (appendix A) that the scalar variance in the free-convection surface layer is independent of z_i, in agreement with existing data.

4. Comparison with observations

Taylor's (1938) "frozen field" hypothesis is typically used to convert measured frequency spectra to streamwise wavenumber spectra. Given a signal $u(t)$ measured at a fixed point, with frequency spectrum $S(f)$ such that

$$\sigma_u^2 = \int_0^\infty S(f)df, \quad (57)$$

to estimate the streamwise wavenumber spectrum $F(\kappa_1)$ one assumes that, in Taylor's words, ". . . the sequence of changes in u at the fixed point is simply due to the passage of an unchanging pattern of turbulent motion over the point. . . ." If so, the streamwise wavenumber and temporal frequency are related by $\kappa_1 = 2\pi f/U$, where U is the mean velocity. Since the wavenumber spectrum also integrates to the variance, one then finds by equating the two integrals that

$$F(\kappa_1) = \frac{U}{2\pi} S\left(\frac{\kappa_1 U}{2\pi}\right). \quad (58)$$

Taylor suggested that his hypothesis requires that ". . . the velocity of the air stream which carries the eddies is very much greater than the turbulent velocity." This is not the usual case with most measurements at fixed points in turbulent shear flows, including tower-based measurements in the atmospheric surface layer. There have been a number of studies of the impact of high-turbulence levels on the validity of Taylor's hypothesis. As discussed by Wyngaard (1986), theoretical (Lumley 1965) and experimental (Deardorff and Willis 1982) work indicates that a high turbulence level increases the amplitude of the inferred wavenumber spectrum at large (inertial range) wavenumbers; that is, it aliases variance to high wavenumbers. Since variance is conserved, the low-wavenumber portions of the spectrum must be attenuated. The measurements of Deardorff and Willis (1982) indicate that the effects on spectral levels can be substantial—on the order of a factor of 2 in some cases. This puts limits on how closely one can compare spectral measurements with models.

The one-dimensional spectra implied by our interpolation models are

$$F^m(\kappa_1) = 2\int_{-\infty}^\infty \frac{E^m(\kappa)}{2\pi\kappa} d\kappa_2. \quad (59)$$

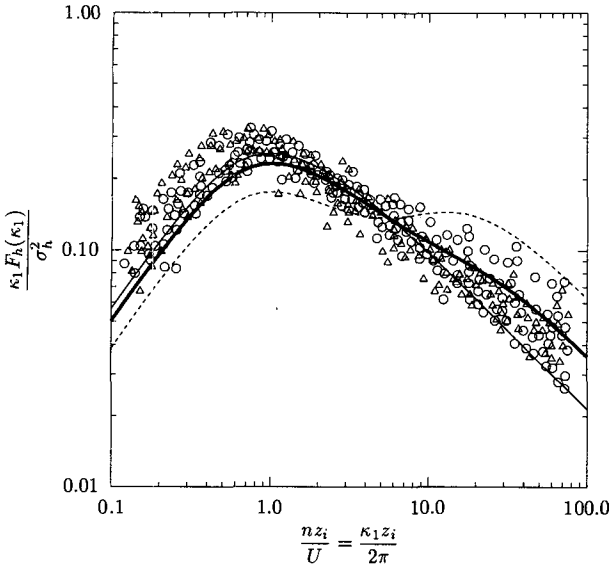

FIG. 2. Modeled one-dimensional horizontal energy spectra compared with Kaimal's (1978) results at $z = 4$ and 32 m from the 1973 Minnesota experiments. Kaimal's data points for the longitudinal velocity (circles) and lateral velocity (triangles) are shown. The curves are the predicted spectra for the average of his cases (heavy solid), his least unstable run ($-z/L = 0.10$, $-z_i/L = 30$; dashed), and his most unstable run ($-z/L = 5.6$, $-z_i/L = 370$; light solid).

We found the one-dimensional spectra of vertical velocity and scalars from (59) by numerical integration. For the horizontal energy spectrum the integration can be done analytically, yielding

$$F_h^m(\kappa_1) = 0.71\left\{\frac{1.6z}{[0.091 + (\kappa_1 z)^2]^{5/6}}\,u_*^2 + \frac{0.85z_i}{[23 + (\kappa_1 z_i)^2]^{5/6}}\,w_*^2\right\}. \quad (60)$$

Figure 2 shows a plot of our model (60) of the one-dimensional horizontal energy spectrum, made dimensionless with σ_h^2 as calculated from (45), versus streamwise wavenumber, made dimensionless with z_i. The curves are our model predictions for the least unstable, most unstable, and the average of the runs analyzed by Kaimal (1978) from the 1973 Minnesota experiments. The individual points on the plot are the spectral data presented by Kaimal. Considering the large scatter usually found in measured spectra and the imprecision of Taylor's frequency–wavenumber conversion at high-turbulence levels, we feel the agreement is quite good.

A different presentation is typically used for the one-dimensional vertical velocity spectrum. Introducing the M–O function for the dissipation rate ϕ_ϵ, defined by

$$\phi_\epsilon = \frac{kz\epsilon}{u_*^3}, \quad (61)$$

yields a dimensionless form of F_{33} that collapses to a single curve in the inertial subrange:

$$\frac{\kappa_1 F_{33}}{u_*^2 \phi_\epsilon^{2/3}} \to \frac{4\alpha_1}{3k^{2/3}}(\kappa_1 z)^{-2/3}. \quad (62)$$

Figure 3 shows our modeled version of F_{33}, scaled as in (62), compared with the measured spectra from the 11 Minnesota runs analyzed by Kaimal (1978). We computed our model spectrum for each of these runs, separated the results into the three stability ranges used by Kaimal, and averaged the spectra in each range. The agreement is very good.

Figure 4 shows a plot of our predicted vertical velocity variance and the Minnesota measurements reported by Kaimal et al. (1976). The curve is a good fit to those data, with the predicted departure from M–O similarity being quite consistent with the measurements.

The analogous M–O scaling for the one-dimensional scalar spectrum yields the inertial-range behavior

$$\frac{\kappa_1 F_c}{C_*^2 \phi_\chi \phi_\epsilon^{-1/3}} \to \frac{\beta_1}{\kappa^{2/3}}(\kappa_1 z)^{-2/3}, \quad (63)$$

where ϕ_χ is the M–O function for the molecular destruction rate of scalar variance,

$$\phi_\chi = \frac{kz\chi}{u_* C_*^2}. \quad (64)$$

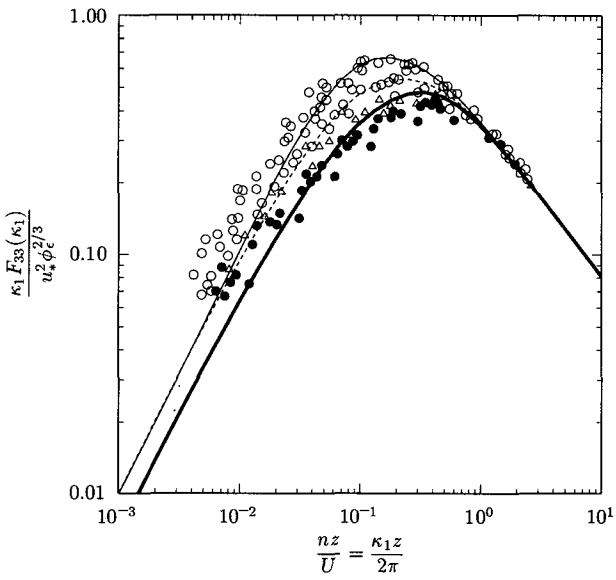

FIG. 3. Modeled one-dimensional vertical velocity spectra compared with Kaimal's (1978) results at $z = 4$ and 32 m from the 1973 Minnesota experiments. Data code: solid circles, $0.1 > -z/L > 0.3$; triangles, $0.3 > -z/L > 0.7$; open circles, $0.7 > -z/L > 6.0$. The heavy solid, dashed, and light solid curves are the averages of our model spectra for the runs falling into those stability ranges, respectively.

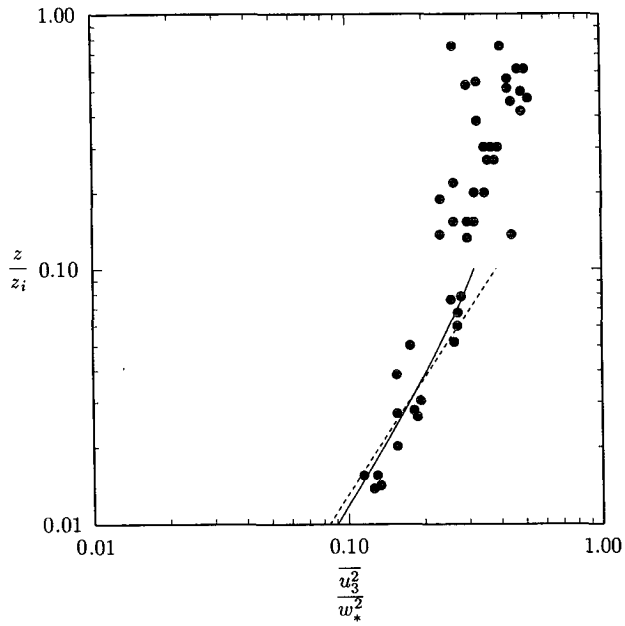

FIG. 4. The height dependence of the vertical velocity variance predicted by (53), solid curve; the Wyngaard et al. (1971) local free-convection fits to the Kansas data, dashed curve; and the Minnesota data (Kaimal et al. 1976), solid circles.

Figure 5 shows our modeled version of F_c scaled as in (63). The temperature and humidity data from Schmitt et al. (1979) and the temperature data from Minnesota 1973, as reported by them, are shown for comparison. The agreement in the inertial range is quite good, as it should be, but in the energy-containing range the fit is less impressive. Two additional reasons for the discrepancies come to mind. First, the temperature field in the atmospheric boundary layer is inherently nonstationary; in convective conditions the temperature flux divergence causes an increase of temperature with time. This could affect the measured frequency spectrum, particularly at the lowest frequencies (largest scales). Second, our spectral model accounts only for that portion of the fluctuating temperature field that is generated through the surface temperature flux. However, scalar fluctuations in the surface layer can also be caused by entrainment at the capping inversion. This additional source of temperature fluctuations could also affect the measured spectral shape in the energy-containing range.

5. Application to LES

Our model of the two-dimensional spectra is directly useful in scaling large-eddy simulation fields. In LES each dependent variable field is decomposed into resolvable and subgrid-scale components denoted by superscripts r and s,

$$f(x_i, t) = f^r(x_i, t) + f^s(x_i, t), \tag{65}$$

the resolvable component being defined as the spatially filtered full field. Thus, each field calculated in large-eddy simulation is resolved up to a filter cutoff wavenumber κ_c, where κ_c is of the order of the reciprocal of the grid spacing Δ. The code of Moeng (1984) uses the Fourier representation in the horizontal with a wave cutoff filter at $\kappa_c = \pi/\Delta$ in that plane; the filtering in the z direction is done by the finite differences used there.

With a wave cutoff filter the variance of a variable is the sum of the variances of its resolvable and subgrid-scale components,

$$\overline{f^2} = \overline{(f^r)^2} + \overline{(f^s)^2}, \tag{66}$$

since nonoverlapping Fourier modes are uncorrelated (Lumley and Panofsky 1964). With a Fourier representation in the horizontal directions the variance of a resolvable-scale field is thus

$$\overline{(f^r)^2} = \int\int_{-\kappa_c}^{\kappa_c} \phi(\kappa_1, \kappa_2) d\kappa_1 d\kappa_2, \tag{67}$$

where ϕ is the spectrum of f. Let us approximate this as an integral of the two-dimensional spectrum:

$$\overline{(f^r)^2} = \int_0^{\kappa_c} E(\kappa) d\kappa. \tag{68}$$

Using our model (26) of the two-dimensional spectrum and the expression (29) for its integral, this yields

$$\frac{\overline{(f^r)^2}}{\overline{f^2}} = 1 - \left[1 \Big/ \left(1 + \frac{(\kappa_c l)^2}{c_2}\right)\right]^{1/3}. \tag{69}$$

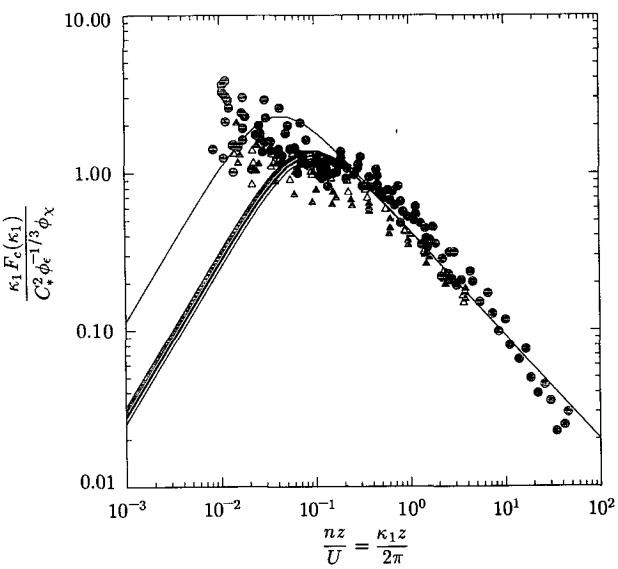

FIG. 5. As in Fig. 2 but for the one-dimensional spectrum of a scalar. The data are temperature (solid triangles) and humidity (open triangles) from the 1973 Minnesota experiments and humidity (solid circles) from the 1974 Pole experiment, as reported by Schmitt et al. (1979).

Using (66), the corresponding expression for the variance of the subgrid-scale field is

$$\frac{\overline{(f^s)^2}}{\overline{f^2}} = \left[1 \Big/ \left(1 + \frac{(\kappa_c l)^2}{c_2}\right)\right]^{1/3}. \quad (70)$$

Thus, according to our surface-layer spectral model, the parameter $(\kappa_c l)^2/c_2$ determines the distribution of the variance into resolvable and subgrid parts in wave cutoff LES. If we define κ_c^* as that cutoff wavenumber at which 50% of the variance is resolved, we have from (69)

$$\kappa_c^* l = \sqrt{7c_2}. \quad (71)$$

Under neutral conditions we used $l = z$, so (71) yields

neutral surface layer:

$$\kappa_c^* z = 0.8, \quad \text{horizontal velocity};$$
$$\kappa_c^* z = 6.0, \quad \text{vertical velocity};$$
$$\kappa_c^* z = 0.6, \quad \text{scalars}. \quad (72)$$

This indicates that roughly an order of magnitude more grid resolution is needed for vertical velocity in the neutral surface layer than is required for scalars or horizontal velocity.

The continuity transfer function complicates the derivation of the corresponding expressions for vertical velocity in the free-convection limit (appendix B). For $z/z_i \ll 1$ and $\kappa_c z \geq 3$, they are approximated well by

$$\frac{\overline{(f^r)^2}}{\overline{f^2}} \approx 1 - 0.7(\kappa_c z)^{-2/3}, \quad (73)$$

$$\frac{\overline{(f^s)^2}}{\overline{f^2}} \approx 0.7(\kappa_c z)^{-2/3}. \quad (74)$$

The expressions for free convection are then

free-convection surface layer:

$$\kappa_c^* z = 12.7\frac{z}{z_i}, \quad \text{horizontal velocity};$$
$$\kappa_c^* z = 1.7, \quad \text{vertical velocity};$$
$$\kappa_c^* z = 1.5, \quad \text{scalars}. \quad (75)$$

The required resolution for horizontal velocity is now independent of z because we modeled those eddies as scaling with z_i. That for vertical velocity continues to depend on z, due to the continuity transfer function, but is less stringent than under neutral conditions; the result for scalars is more stringent than under neutral conditions.

Figure 6 shows our model spectra for horizontal energy, vertical velocity, and scalars near the surface under neutrally stable, slightly convective, and free-convective conditions; κ_c^* is indicated by the vertical lines.

6. Summary

We have presented an approach to modeling the spectra of velocity components and transported scalars in the atmospheric surface layer. Rather than modeling one-dimensional spectra, as has been traditionally done, we model the two-dimensional spectra in the horizontal plane. This allows us to incorporate the important physical constraints of horizontal isotropy and continuity. The former is important in free convection, and the latter links the spectrum of vertical velocity to that of horizontal energy.

We use one spectral form for all variables. It has two free constants: one intensity scale and one length scale. We choose these four parameters separately in the neutral and free-convection limits. At neutral we use law-of-the-wall scaling; in free convection we use mixed-layer scaling. Our vertical velocity spectrum in free convection is the product of a continuity transfer function and the horizontal energy spectrum; as such, it has no free constants and is not constrained to follow M–O similarity. We then model the stability dependence of the velocity spectra by adding the spectra in the neutral and free-convection limits. We show that for scalars it is necessary to add these spectra in parallel.

The resulting spectra agree well with observations from Minnesota. Our expression for the variance of horizontal energy as a function of stability agrees with observed behavior. Remarkably, the predicted vertical velocity variance displays the observed local free-convection asymptote of M–O similarity near the surface

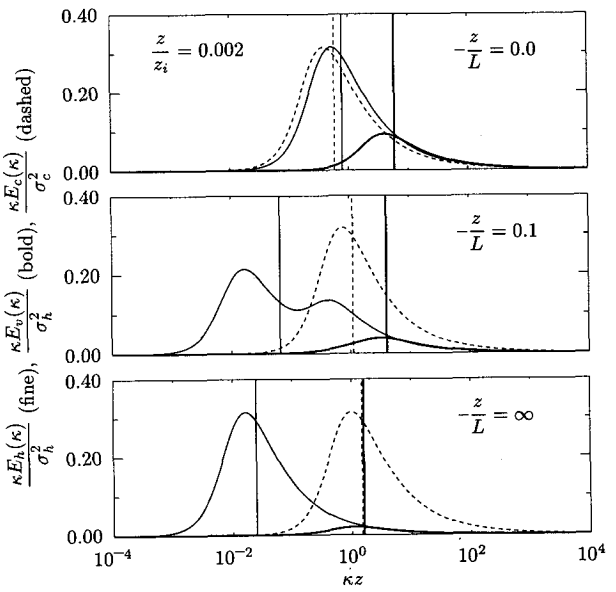

FIG. 6. Near-surface ($z/z_i = 0.002$) spectra of horizontal energy (fine), vertical velocity (bold), and scalars (dashed) under neutrally stable ($-z/L = 0.0$), slightly convective ($-z/L = 0.1$), and free-convective ($-z/L = \infty$) conditions. The vertical lines show κ_c^*, the cutoff wavenumber at which 50% of the variance is resolved.

and a realistic departure from M–O similarity at greater heights. Adequate data seem not to exist to test our predictions for the scalar spectrum. The tests we could make with temperature data do not show strong agreement, perhaps because of the effects of trends on temperature fluctuations. Better data on scalar spectra in the surface layer are clearly needed.

We used our model two-dimensional spectra to estimate the variance contained in the resolvable scales of LES within the surface layer. Such results are immediately useful in determining grid-resolution requirements for LES. This is also a first step toward the scaling of LES budgets, whose understanding is central to the development of better subgrid and boundary condition models for LES.

Acknowledgments. The authors are grateful to Drs. Chin-Hoh Moeng and Peter Sullivan of NCAR for providing LES data on free convection. Financial support was provided by U.S. Army Research Office Grant #DAAL03-92-G-0117 and by Office of Naval Research Grant #N00014-92-J-1688.

APPENDIX A

Determining the Spectral Constants

a. The horizontal energy spectrum

The neutral turbulent kinetic energy (TKE) budget reduces to a near-balance between shear production and viscous dissipation (Tennekes and Lumley 1972). Thus, at neutral we have $\epsilon = u_*^3/kz$, where $k \approx 0.4$ is the von Kármán constant. We choose $l = z$, $s = u_*$. The one-dimensional spectral constant α_1 has been measured in numerous flows, including the atmospheric surface layer, and arguments can be made for values in the range from 0.48 to about 0.56. If we take $\alpha_1 = 0.52$, (37) then yields

$$c_1^n \approx 1.6. \tag{A1}$$

Taking $\sigma_h^2 = (\overline{u_1^2} + \overline{u_2^2})/2 \approx 12^{2/3} u_*^2$ at neutral (Kaimal 1978), (29) then yields

$$c_2^n \approx 0.090. \tag{A2}$$

The TKE budget under very unstable conditions shows strong evidence of approaching a state where the loss from turbulent transport to higher levels balances the gain from pressure transport, while the gain from buoyant production balances the loss to viscous dissipation (Wyngaard 1992). This balance is consistent with surface-layer measurements in free convection (Deardorff and Willis 1985). Thus, in free convection we take $\epsilon \approx gQ_0/T_0 = w_*^3/z_i$. With $l = z_i$, $s = w_*$, (37) then gives

$$c_1^f \approx 0.85. \tag{A3}$$

Using $\sigma_h^2 \approx 0.45 w_*^2$ in free convection (Deardorff and Willis 1985) then gives from (29)

$$c_2^f \approx 23. \tag{A4}$$

b. The vertical velocity spectrum

For vertical velocity in the neutral surface layer, the inertial-range constraint (37) becomes, using $\epsilon = u_*^3/(kz)$,

$$c_1^n = \frac{4\alpha_1}{3(0.71)} \left(\frac{\epsilon z}{u_*^3}\right)^{2/3} \approx 1.8. \tag{A5}$$

With $\overline{u_3^2}^f \approx 1.55 u_*^2$ (Panofsky and Dutton 1984), (29) then implies

$$c_2^n \approx 5.2. \tag{A6}$$

From (28) and (43) our form for E_v^f is

$$E_v^f = \frac{(\kappa z)^2}{\left[\frac{1}{2A^2} + \frac{7}{8}(\kappa z)^2\right]} \frac{0.85 z_i^2 \kappa}{[23 + (\kappa z_i)^2]^{4/3}} w_*^2. \tag{A7}$$

A complicated, analytic integration yields for $z \ll z_i$ [(B3) and (B4), appendix B]

$$\overline{u_3^2}^f = \int_0^\infty E_v^f(\kappa) d\kappa = 1.69(2A^2)^{1/3} \left(\frac{z}{z_i}\right)^{2/3} w_*^2 = 1.69(2A^2)^{1/3} u_f^2, \tag{A8}$$

where $u_f = (gQ_0 z/T_0)^{1/3}$ is the local-free-convection velocity scale. The parameter A, defined in (13), typically lies in the range $0.8 < A < 1.0$. If we take $A = 0.9$ as representative, then (A8) gives

$$\overline{u_3^2}^f = 2.0 u_f^2. \tag{A9}$$

Observations of true free convection in the atmospheric surface layer are rare, but under very unstable conditions $\overline{u_3^2}$ is observed to behave as

$$\overline{u_3^2} \approx u_*^2 \left(-\frac{z}{L}\right)^{2/3}. \tag{A10}$$

We can rewrite this as

$$\overline{u_3^2} = C u_f^2. \tag{A11}$$

The constant C has been reported as 1.7 (Panofsky and Dutton 1984), 2.0 (Wyngaard et al. 1971), and 2.6 (Monji 1973). Our result (A9) lies within this range.

c. The scalar spectrum

In the neutral surface layer (Wyngaard and Coté 1971)

$$\chi \approx -2\overline{wc} \frac{\partial C}{\partial z} = 2u_* C_* \frac{C_*}{kz} \phi_h(0) = 2 \frac{u_* C_*^2}{kz} 0.74 = \frac{1.5 u_* C_*^2}{kz}. \tag{A12}$$

For the variance we take

$$\overline{c^2} = 6.25C_*^2, \tag{A13}$$

which is consistent with Panofsky and Dutton (1984, p. 171). With $\beta_1 = 0.4$, $l = z$, and $\epsilon = u_*^3/kz$, this yields from (37) and (29)

$$c_1^n \approx 1.5, \quad c_2^n \approx 0.05. \tag{A14}$$

In free convection we assume that scalar statistics follow the asymptotes suggested by observations of temperature in the very unstable surface layer. For variance we write (Wyngaard et al. 1971)

$$\overline{c^2} \approx 0.9C_*^2\left(-\frac{z}{L}\right)^{-2/3} = 1.66C_f^2. \tag{A15}$$

In very unstable conditions a local free-convection fit to the scalar gradient is (Businger 1973)

$$\frac{\partial C}{\partial z} \approx \frac{0.2C_*}{kz}\left(-\frac{z}{L}\right)^{-1/3} = \frac{-0.68C_f}{z}. \tag{A16}$$

We can then write

$$\chi \approx -2\overline{wc}\frac{\partial C}{\partial z} = \frac{1.36u_fC_f^2}{z}, \tag{A17}$$

so that with $\epsilon \approx gQ_0/T_0$ and $l = z_i$ we have from (37) and (29)

$$c_1^f = 0.77\left(\frac{z}{z_i}\right)^{-2/3}, \quad c_2^f \approx 0.34\left(\frac{z}{z_i}\right)^{-2}. \tag{A18}$$

APPENDIX B

The Vertical Velocity Variance

The variance of resolvable-scale vertical velocity is, from (50) and (68),

$$\begin{aligned}\overline{(u_3^r)^2} &= \int_0^{\kappa_c}[E_v^n(\kappa) + T(\kappa, z)E_h^f(\kappa)]d\kappa \\ &= \int_0^{\kappa_c}E_v^n(\kappa)d\kappa + \int_0^{\kappa_c}T(\kappa)E_h^f(\kappa)d\kappa \\ &= \overline{(u_3^r)^2}^n + \overline{(u_3^r)^2}^f. \end{aligned}\tag{B1}$$

Evaluating the neutral contribution is straightforward, as shown in section 5. The free-convection contribution is, from (52),

$$\begin{aligned}\overline{(u_3^r)^2}^f &= \int_0^{\kappa_c}\frac{(\kappa z)^2}{\left[0.62 + \frac{7}{8}(\kappa z)^2\right]} \\ &\quad\times\frac{0.85z^2\kappa}{[23(z/z_i)^2 + (\kappa z)^2]^{4/3}}u_f^2d\kappa \\ &= \frac{c}{a^{1/3}}\int_0^{x_c}\frac{x}{(1+x)}\frac{dx}{(\epsilon + x)^{4/3}}, \end{aligned}\tag{B2}$$

where $a = 8(0.62)/7$, $c = 4(0.85)u_f^2/7$, $x = (\kappa z)^2/a$, $\epsilon = 23(z/z_i)^2/a$, and $x_c = (\kappa_c z)^2/a$. Letting $X = [(1-\epsilon)/(\epsilon + x_c)]^{1/3}$ and $Y = [(1-\epsilon)/\epsilon]^{1/3}$, (B2) yields

$$\begin{aligned}\overline{(u_3^r)^2}^f &= \frac{c}{2}a^{-1/3}(1-\epsilon)^{-4/3} \\ &\quad\times\left\{6\epsilon(X-Y) - 2\sqrt{3}\left[\tan^{-1}\left(\frac{2X-1}{\sqrt{3}}\right)\right.\right. \\ &\quad\left.\left. - \tan^{-1}\left(\frac{2Y-1}{\sqrt{3}}\right)\right] + \ln\left[\frac{X^2 - X + 1}{(X+1)^2}\right]\right. \\ &\quad\left. - \ln\left[\frac{Y^2 - Y + 1}{(Y+1)^2}\right]\right\}. \end{aligned}\tag{B3}$$

We can simplify (B3) by recognizing that it contains two small parameters. In the surface layer $z \ll z_i$, so ϵ is small. The cutoff wavenumber $\kappa_c \approx 1/\Delta$, where Δ is the grid mesh size [in Moeng's (1984) LES code $\kappa_c = \pi/\Delta$]. Let us assume that $\Delta \sim z$, so that x_c^{-1} is the second small parameter. Expanding (B3) in Taylor series about $\epsilon = 0$, $x_c^{-1} = 0$ gives

$$\begin{aligned}\overline{(u_3^r)^2}^f &\approx \frac{c}{2}a^{-1/3}\left[\frac{\pi}{\sqrt{3}} + \sqrt{3}\pi - 9\epsilon^{2/3} - 6x_c^{-1/3}\right] \\ &= \left[2.0 - 25\left(\frac{z}{z_i}\right)^{4/3} - 1.4(\kappa_c z)^{-2/3}\right]u_f^2. \end{aligned}\tag{B4}$$

For $(\kappa_c z) > 2.5$ and $z/z_i < 0.03$, the difference between (B3) and (B4) is less than 10%.

REFERENCES

Batchelor, G. K., 1960: *Homogeneous Turbulence.* Cambridge University Press, 197 pp.

Businger, J., 1973: Turbulent transfer in the atmospheric surface layer. *Workshop on Micrometeorology,* D. A. Haugen, Ed., Amer. Meteor. Soc., 67–100.

Deardorff, J. W., and G. E. Willis, 1982: Investigation of the frozen-turbulence hypothesis for temperature spectra in a convectively mixed layer. *Phys. Fluids,* **25,** 21–28.

——, and ——, 1985: Further results from a laboratory model of the convective planetary boundary layer. *Bound.-Layer Meteor.,* **32,** 205–236.

Højstrup, J., 1982: Velocity spectra in the unstable planetary boundary layer. *J. Atmos. Sci.,* **39,** 2239–2248.

Kaimal, J. C., 1978: Horizontal velocity spectra in an unstable surface layer. *J. Atmos. Sci.,* **35,** 18–24.

——, J. C. Wyngaard, D. A. Haugen, O. R. Coté, and Y. Izumi, 1976: Turbulence structure in the convective boundary layer. *J. Atmos. Sci.,* **33,** 2152–2169.

Kristensen, L., D. H. Lenschow, P. Kirkegaard, and M. Courtney, 1989: The spectral velocity tensor for homogeneous boundary-layer turbulence. *Bound.-Layer Meteor.,* **47,** 149–193.

Lumley, J. L., 1965: Interpretation of time spectra measured in high-intensity shear flows. *Phys. Fluids,* **8,** 1056–1062.

——, and H. A. Panofsky, 1964: *The Structure of Atmospheric Turbulence.* Interscience, 239 pp.

Mann, J., 1994: The spatial structure of neutral atmospheric surface layer turbulence. *J. Fluid Mech.,* **273,** 141–168.

Moeng, C.-H., 1984: A large-eddy-simulation model for the study of planetary boundary-layer turbulence. *J. Atmos. Sci.,* **41,** 2052–2062.

Monji, N., 1973: Budgets of turbulent kinetic energy and temperature variance in the transition zone from forced to free convection. *J. Meteor. Soc. Japan,* **51,** 133–145.

Panofsky, H. A., and J. A. Dutton, 1984: *Atmospheric Turbulence.* John Wiley & Sons, 397 pp.

——, H. Tennekes, D. H. Lenschow, and J. C. Wyngaard, 1977: The characteristics of turbulent velocity components in the surface layer under convective conditions. *Bound.-Layer Meteor.,* **11,** 355–361.

Paulson, C. A., 1970: The mathematical representation of wind speed and temperature profiles in the unstable atmospheric surface layer. *J. Appl. Meteor.,* **9,** 857–861.

Robertson, H. P., 1940: The invariant theory of isotropic turbulence. *Proc. Camb. Philos. Soc.,* **36,** 209–223.

Schmitt, K. F., C. A. Friehe, and C. H. Gibson, 1979: Structure of marine surface layer turbulence. *J. Atmos. Sci.,* **36,** 602–618.

Taylor, G. I., 1938: The spectrum of turbulence. *Proc. Roy. Soc. London, Ser. A.,* **164,** 476–490.

Tennekes, H., and J. L. Lumley, 1972: *A First Course in Turbulence.* MIT Press, 300 pp.

von Kármán, T., 1948: Progress in the statistical theory of turbulence. *Proc. Natl. Acad. Sci.,* **34,** 530–539.

Willis, G. E., and J. W. Deardorff, 1974: A laboratory model of the unstable planetary boundary layer. *J. Atmos. Sci.,* **31,** 1297–1307.

Wyngaard, J. C., 1986: Measurement physics. *Probing the Atmospheric Boundary Layer,* D. H. Lenschow, Ed., Amer. Meteor. Soc., 5–18.

——, 1988: Structure of the PBL. *Lectures on Air Pollution Modeling,* A. Venkatram and J. C. Wyngaard, Eds., Amer. Meteor. Soc., 9–61.

——, 1992: Atmospheric turbulence. *Annu. Rev. Fluid Mech.,* **24,** 205–233.

——, and O. R. Coté, 1971: The budgets of turbulent kinetic energy and temperature variance in the atmospheric surface layer. *J. Atmos. Sci.,* **28,** 222–233.

——, ——, and Y. Izumi, 1971: Local free convection, similarity, and the budgets of shear stress and heat flux. *J. Atmos. Sci.,* **28,** 1171–1182.